A&A 435, 353–362 (2005)
DOI: 10.1051/0004-6361:20042482

Astronomy & Astrophysics

Near-infrared (0.8–4.0 μm) spectroscopy of Mimas, Enceladus, Tethys, and Rhea

J. P. Emery[1,⋆], D. M. Burr[2], D. P. Cruikshank[3], R. H. Brown[4], and J. B. Dalton[5]

[1] NASA Ames Research Center/SETI Institute, Mail Stop 245-6, Moffett Field, CA 94035, USA
e-mail: jemery@mail.arc.nasa.gov
[2] USGS Astrogeology Branch, 2255 N Gemini Dr, Flagstaff, AZ 86001, USA
[3] NASA Ames Research Center, Mail Stop 245-6, Moffett Field, CA 94035, USA
[4] Lunar and Planetary Laboratory, Univ. of Arizona, 1629 E. University Dr, Tucson, AZ 85721, USA
[5] NASA Ames Research Center/SETI Institute, Mail Stop 245-3, Moffett Field, CA 94035, USA

Received 3 December 2004 / Accepted 25 January 2005

Abstract. Spectral measurements from the ground in the time leading up to the Cassini mission at Saturn provide important context for the interpretation of the forthcoming spacecraft data. Whereas ground-based observations cannot begin to approach the spatial scales Cassini will achieve, they do possess the benefits of better spectral resolution, a broader possible time baseline, and unique veiewing geometries not obtained by spacecraft (i.e., opposition). In this spirit, we present recent NIR reflectance spectra of four icy satellites of Saturn measured with the SpeX instrument at the IRTF. These measurements cover the range 0.8–4.0 μm of both the leading and trailing sides of Tethys and the leading side of Rhea. The L-band region (2.8–4.0 μm) offers new opportunities for searches of minor components on these objects. Additionally, these data include 0.8–2.5 μm spectra of both the leading and trailing sides of Mimas and of the (mostly) trailing side of Enceladus. The spectrum of Enceladus shows activity near 2.25 μm that we interpret as a possible signature of NH_3 ice. The presence of ammonia in the Saturn system is not unexpected, and may help explain the apparent recent geologic activity of Enceladus. Analysis of leading/trailing differences in H_2O band depths, spectral slopes, and albedo imply a separate regime of surface modification for Mimas and Enceladus than for the more distant icy satellites (Tethys, Dione, Rhea). Aside from the potential NH_3 on Enceladus, no other minor constituents are detected in these icy surfaces.

Key words. planets and satellites: individual: Enceladus – planets and satellites: individual: Mimas – infrared: solar system – planets and satellites: individual: Rhea – planets and satellites: individual: Tethys – planets and satellites: general

1. Introduction

The Cassini spacecraft is currently in orbit around Saturn, and has already imaged all the major satellites. This mission is providing the first close-up look at the system since the Voyagers flew by in 1980 and 1981. Over the next 4+ years, the VIMS instrument will obtain visible and near-infrared (NIR) spectra of the icy satellites. Those observations will be spatially resolved and will for the first time be able to address the possibility of compositionally distinct units on the surfaces. Whereas ground-based observations cannot begin to approach such spatial scales, they do possess the benefits of better spectral resolution, a broader possible time baseline, and unique viewing geometries. Spectral measurements from the ground in the time leading up to the Cassini mission at Saturn provide useful context for the interpretation of the forthcoming spacecraft data.

The H_2O ice nature of the surfaces of the larger icy satellites (Tethys, Dione, Rhea, and the trailing side of Iapetus) was discovered in the mid-1970s with the use of broadband photometry (Johnson et al. 1975; Morrison et al. 1976). Spectroscopy quickly followed, revealing H_2O on some of the other moons (Hyperion, Enceladus, and eventually Mimas and Phoebe) and providing a better understanding of the nature of the ice on these surfaces (e.g., Fink et al. 1976; Cruikshank 1980; Cruikshank & Brown 1982; Owen et al. 1999). Clark et al. (1984b) presented an in-depth spectral analysis of the system, recording 0.8–2.5 μm spectra of both the leading and trailing sides of the major satellites. Through an analysis of the relative depths of the various H_2O ice bands, they concluded that the surfaces are nearly pure H_2O ice with <1 wt% particulates averaged on a global scale. Grundy et al. (1999) presented updated spectra covering similar wavelengths with much better signal-to-noise ratio (S/N). They used the behavior of the temperature-sensitive 1.65-μm absorption feature in crystalline H_2O to estimate surface temperatures from their data. Taking advantage of reduced glare from the rings during ring-plane crossing, Buratti et al. (1998) and Momary et al. (2000) performed photometry of many of Saturns icy satellites in the infrared, from which they derived geometric albedos. Most recently, Cruikshank et al. (2005) present spectra of all the large

⋆ Visiting astronomer, NASA Infrared Telescope Facility.

icy satellites and extend the spectral coverage of the trailing side of Dione and the leading side of Rhea to 3.6 μm.

The surface composition of Saturn's icy satellites, and the differences among them, are related both to their intrinsic make up and to their geologic and environmental histories. The Voyager images of these icy worlds show evidence for post-accretional and post-heavy-bombardment geological activity throughout the Saturnian system (e.g., Morisson et al. 1986; Squyres & Croft 1986, and references therein). Enceladus shows the most dramatic evidence for very recent activity, containing at least five discrete geologic units – one of these is completely devoid of impact craters at Voyager resolutions – and displaying cross-cutting relationships among the units and related ridges and troughs. Furthermore, Enceladus orbits within Saturns E-ring, which has a maximum density near this moon. The dynamical lifetime of these ring particles is quite short ($\sim 10^4$ yr, Haff et al. 1983), which raises speculation that current activity on Enceladus may be actively or episodically repopulating the E-ring. Crater distributions also provide strong evidence for regions of varying ages on each of the major icy satellites. Along with this, the cratering analysis of Plescia & Boyce (1982, 1983) indicate two different populations of impactors, perhaps one heliocentric and one Saturn-centric.

This geologic activity is somewhat hard to explain. Ellsworth & Shubert (1983) studied conductive and convective energy transport in the interiors of the Saturnian satellites and concluded that radiogenic and accretional heating do not supply enough energy to drive geologic activity in H_2O ice. None of these satellites are in orbital resonances that would induce sufficient tidal heating to drive geologic activity (Greenberg 1984), as occurs on Io and Europa. Ammonia and/or ammonia hydrates would lower melting temperatures if included with H_2O in sufficient quantities. Though this remains a possible explanation for the apparently recent activity, no evidence for these materials has been detected in previous spectra of these surfaces.

Voyager Plasma Science and Low Energy Charged Particle observations, along with those of the Pioneer 11 plasma analyzer, revealed that the Saturnian magnetosphere contains abundant ions, with "clouds" of dominant species existing at different Saturn-centric distances (Frank et al. 1980; Bridge et al. 1981, 1982; Krimigis et al. 1983; Eviatar 1984). Delitsky & Lane (2002) have predicted the surface chemistry that should be induced as these ions impact satellite surfaces. Measured abundances (or upper limits) of these species can be used to investigate the importance of magnetosphere-surface interactions on the modification of the surfaces of icy Saturnian satellites.

We present near-infrared reflectance spectra of four moons of Saturn. These new data of Tethys and Rhea extend from 0.8 to 4.1 μm and cover both the leading and trailing hemispheres of Tethys and the leading hemisphere of Rhea. The data for Mimas and Enceladus extend from 0.8 to 2.5 μm and cover both the leading and trailing hemispheres of Mimas and the trailing hemisphere of Enceladus. The analysis in this paper consists mainly of comparisons among the spectra and with previously published data and a search for minor components. A follow-on paper (Dalton et al. in preparation) will present a more quantitatively rigorous analysis of the H_2O ice bands.

2. Observations

Observations were made at the NASA Infrared Telescope Facility (IRTF) atop Mauna Kea, Hawaii. All spectra were collected with the medium resolution near-infrared spectrograph/imager SpeX (Rayner et al. 1998). This instrument contains two detectors: a 1024×1024 InSb array for the spectrograph and a 512×512 InSb array which images the slit. The slit imager is used for guiding the telescope by characterizing the spillover of the PSF outside the slit. SpeX has several available observing modes. We used the short wavelength cross-dispersed (SXD) mode to acquire spectra from 0.8 to 2.4 μm and the long wavelength cross-dispersed (LXD) mode to acquire spectra from 1.9 to 4.1 μm. By stacking six orders on the spectrograph detector, the entire wavelength range for a given mode is measured simultaneously. Using a 0.8×15 arcsec slit with an image scale of 0.15 arcsec/pixel provides a spectral resolution ($R = \lambda/\Delta\lambda$) of ~800 for the LXD mode and ~650 for the SXD mode.

Data frames were taken in pairs with the object dithered along the slit. Subtraction of these pairs produces a first order removal of sky emission. The maximum on-chip integration time in *IJHK*-bands is ~120 s to minimize the effects of variability of the sky emission. The maximum integration time in *L*-band is shorter (~30 s) due to high thermal background and more rapid sky variability. Typically, multiple frames are taken with the maximum on-chip integration time and summed together during data reduction in order to increase the signal-to-noise ratio (S/N). Nearby solar analogue stars were observed regularly throughout the satellite observations to ensure good correction of atmospheric absorption and solar spectral slope. With SpeX, flat field images are obtained by illuminating an integrating sphere which is in a calibration box attached to the spectrograph. This box also contains an argon lamp that is used for wavelength calibration. For more details of our observing and data reduction procedures, see Emery (2002) and Emery & Brown (2003).

These Saturnian satellites were observed as serendipitous targets during other programs (when the program objects were not observable), so the observation dates stretch over a year and half (from October 2001 to April 2003). Also because of this, the observations are typically somewhat intermediate between leading (90° longitude) and trailing (270° longitude) hemispheres rather than being precisely targeted at one or the other. Table 1 lists the dates and other observation parameters for each object. We have scaled the data to the 0.9 μm geometric albedos measured by Buratti et al. (1998); these albedos are also listed in Table 1. The LXD data of Tethys and Rhea are scaled to the SXD data in the overlapping *K*-band region. Buratti et al. did not present an albedo for the leading side of Mimas. Verbiscer & Veverka (1992) find from Voyager clear filter (0.47 μm) photometry that the trailing side of this moon is about 6% brighter than the leading side. Combining this variation with the trailing side albedo given by Buratti et al. (1998), we adopt a value of 0.68 for the geometric albedo of the

Table 1. Observation parameters.

Object	p^a	t_{int} (s)	λ–range (μm)	Date	UT time (midexpos.)	Sub–$\bigoplus$ longitude	Leading/ Trailing	Comparison Star	Type	$B-V$
Mimas	0.68[b]	480	0.8–2.5	7 Apr. 2003	06:38	55	Leading	SAO 77189	G5	0.65
	0.72	960	0.8–2.5	17 Oct. 2001	14:32	266	Trailing	SAO 94332	G4V	0.65
Enceladus	1.02	1140	0.8–2.5	5 Apr. 2003	06:08	320	Interm. (T)	SAO 77189	G5	0.65
Tethys	0.90	480	0.8–2.5	7 Mar. 2002	05:50	68	Leading	SAO 76712	G2V	0.65
		1050	1.9–4.1	7 Mar. 2002	06:33	74	Leading	same		
	0.76	480	0.8–2.5	17 Oct. 2001	14:12	240	Trailing	SAO 94332	G4V	0.65
		760	1.9–4.1	17 Oct. 2001	15:25	249	Trailing	same		
Rhea	0.76	120	0.8–2.5	16 Oct. 2001	15:30	35	Interm. (L)	SAO 94332	G4V	0.65
		1340	1.9–4.1	16 Oct. 2001	13:45	30	Interm. (L)	same		

[a] Geometric albedo at 0.9 μm, from Buratti et al. (1998).
[b] Not given in Buratti et al., so we used the trailing side albedo scaled by the visible light curve. See text.

leading side of Mimas, with the caution that this number could be in error if the lightcurve at 0.9 μm varies substantially from that at 0.47 μm. The Mimas and Enceladus data are also shown in Cruikshank et al. (2005), but are included here with additional analysis and discussion. The spectra of all four objects are presented in Fig. 1.

3. Analysis

The analysis performed in this paper consists of qualitative comparisons among these data (particularly leading/trailing hemispheres of the same object) and with previously published data, analysis of H_2O band depths, and searches for minor components. More detailed investigation of the H_2O bands to constrain physical parameters of these surfaces will be presented in a follow-on paper (Dalton et al. in preparation).

Depths of the H_2O bands are a reasonably good marker of grain size of the ice particles and contamination by non-ice components (e.g., Clark et al. 1984b). They also provide a ready means of comparison with previous data. H_2O ice has five significant absorption bands in the wavelengths studied here: O−H stretching fundamentals at 3 μm and various overtones and combinations at 2.02, 1.52, 1.25, and 1.04 μm. We have adopted the band centers, inter-band positions, and band depth definition of Clark et al. (1984b). The depth is defined relative to a continuum by the equation $D = 1 - R_b/R_c$, where R_b is the reflectance in the center of the band and R_c is the continuum reflectance at the same wavelength. The continuum used is a cubic spline fit to six points outside of the absorption bands (0.95, 1.12, 1.38, 1.78, 2.24, and 3.6 μm). The results are listed in Table 2 and are discussed more below.

Along with searching for minor species, we estimate upper limits on the abundances of several ices (NH_3, CO_2, CH_4, and CO) using Hapke's theory for scattering in a particulate medium (cf. Hapke 1993). To do this, we first fit a pure water ice spectrum to the region of our data under study (typically K-band for these ices). We then add small amounts of the ice under study, until the absorption from that ice becomes larger than the noise in the data. The surface grains are assumed to be in a salt and pepper type mixture, where each grain is a single composition, but a photon may encounter several grains (possibly of different compositions) within the regolith. Since absorption band strengths are dependent on grain size, we estimated limits for both small (12.5 μm) and large (200 μm) grains. The results for each satellite are presented in Table 3 and are discussed below.

Table 2. Water ice band depths[a].

Object	1.04 μm	1.25 μm	1.52 μm	2.02 μm	3.0 μm
Mimas (L)	<0.01	0.063	0.50	0.65	–
(T)	<0.005	0.033	0.43	0.59	–
Enceladus (T)	0.014	0.034	0.47	0.64	–
Tethys (L)	0.006	0.046	0.50	0.63	0.99
(T)	0.014	0.040	0.46	0.61	0.96
Rhea (L)	–	<0.005[b]	0.37[b]	0.61	0.99

[a] Probable errors of band depth measurements are estimated to be ∼0.005. Exceptions are the 1.04-μm band on the leading side of Mimas and the 3-μm band of Tethys and Rhea, where the S/N of the data is lower and errors can reach ∼0.01.
[b] May be compromised by a possible systematic error in the Rhea SXD data. See text.

3.1. Mimas

Mimas is the smallest (R = 197 km) and inner-most of the classical Saturnian satellites, orbiting just outside of the A ring. It is heavily cratered (including the 130 km diameter Herschel on the leading side), with the individual craters showing no evidence of viscous relaxation. The crater counts of Plescia & Boyce (1982) indicate the mixing of two crater populations, which suggests some (ancient) modification of the surface after formation and heavy bombardment. In independent examinations of Voyager imagery, Buratti et al. (1990) and Verbiscer & Veverka (1992) find the surface properties of Mimas to be quite uniform. Their works revealed no albedo or color variations larger than ∼10%.

The photometric uniformity of Mimas for the most part extends to its spectral appearance as well. Figure 1a shows that the leading and trailing side spectra are quite similar. They are both flatter at $\lambda < 1.4$ μm than Enceladus or Tethys. On closer inspection, some leading/trailing differences do appear. The H_2O bands on the leading side are deeper than on the trailing side. The 1.52- and 2.02-μm bands are about 10% deeper on the leading side, and the 1.25-μm band is almost twice as deep (Table 2). A similar trend is described by Clark et al. (1984b) for the Galilean satellites, Tethys, Dione, and Rhea for the

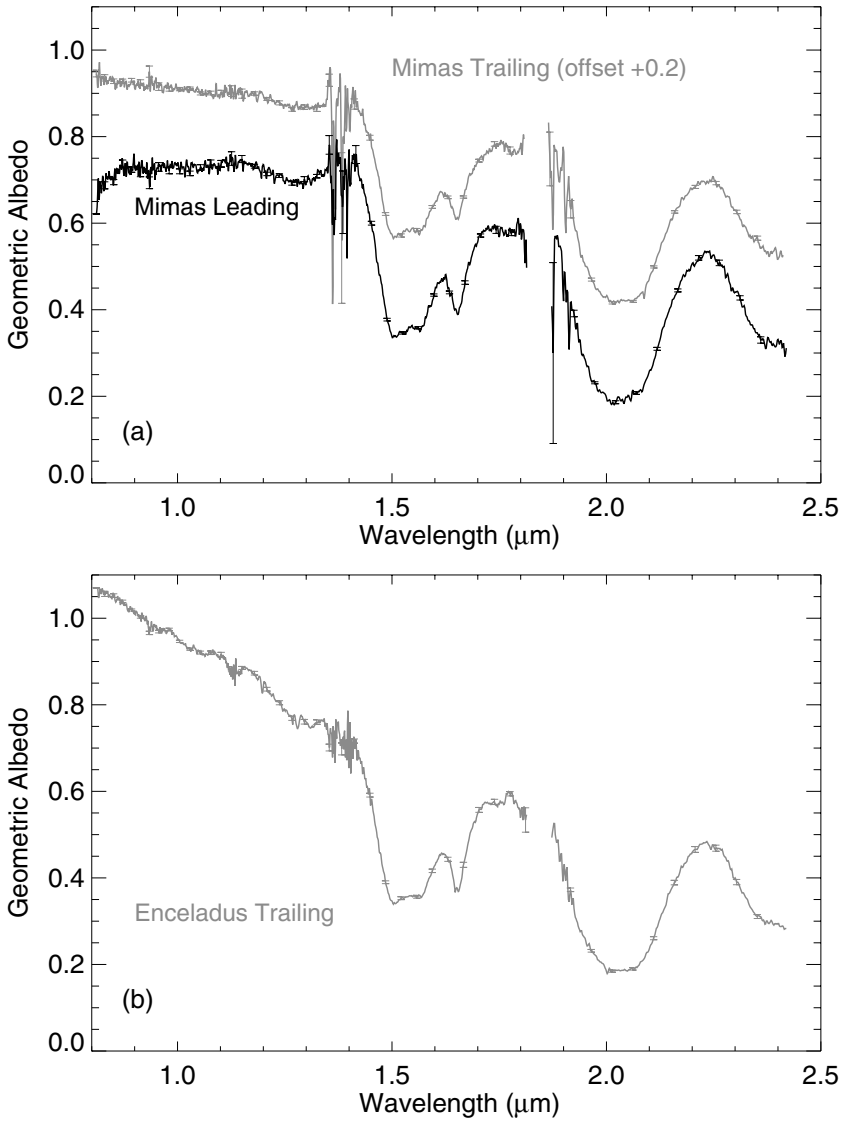

Fig. 1. Near-infrared spectra of four icy satellites of Saturn. All data are scaled to the geometric albedos at 0.9 μm reported by Buratti et al. (1998), except for the leading side of Mimas (see text). The trailing hemisphere spectra of Mimas and Tethys are offset by 0.2 and 0.3, respectively, for clarity. Several representative error bars (about every 30th data point) are shown for each spectrum.

1.52- and 2.02-μm bands, but the Galilean satellites show the opposite trend for the 1.25-μm band. The spectrum of the leading side of Mimas also appears to be slightly flatter at $\lambda < 1.4$ μm than the trailing side spectrum.

There is no indication of any species other than H_2O ice in the spectra of Mimas. The S/N of these spectra is the lowest of our data at $\lambda < 2.5$ μm, so constraints on abundances (Table 3) are not as strict as for the other objects we observed. There can be no more than about 3 wt% of NH_3 on Mimas. CO_2, on the other hand, could comprise as much as 25 wt% (with large grains) and still remain undetected in these data.

3.2. Enceladus

Enceladus is the most geologically interesting of these satellites, showing signs of recent activity. It is the next satellite going outward from Mimas and is slightly larger (R = 251 km) than Mimas. This is the most reflective known airless body in the Solar System (Buratti & Veverka 1984). Voyager imagery shows five distinct terrains on Enceladus, which vary from showing similar crater densities as the other satellites to being entirely devoid of craters at Voyager resolution. These areas with a complete absence of craters suggest a resurfacing event in the recent history for this moon. Equally intriguing, some regions containing similar crater densities exhibit differing viscous relaxation states of their craters (Passey 1983), implying (historical?) variations in heat flow from one unit to the other. Despite such heterogeneity in surface terrain, the photometric properties of Enceladus are remarkably uniform across the surface, which (combined with the high albedo and flat visible spectrum) may suggest a surface veneer of pure H_2O covering all terrain units (e.g. Buratti et al. 1990). Enceladus orbits within Saturn's E-ring, which extends from 4 to 8 R_S. Photometric studies of this ring indicate very small ($D \sim 1$ μm,

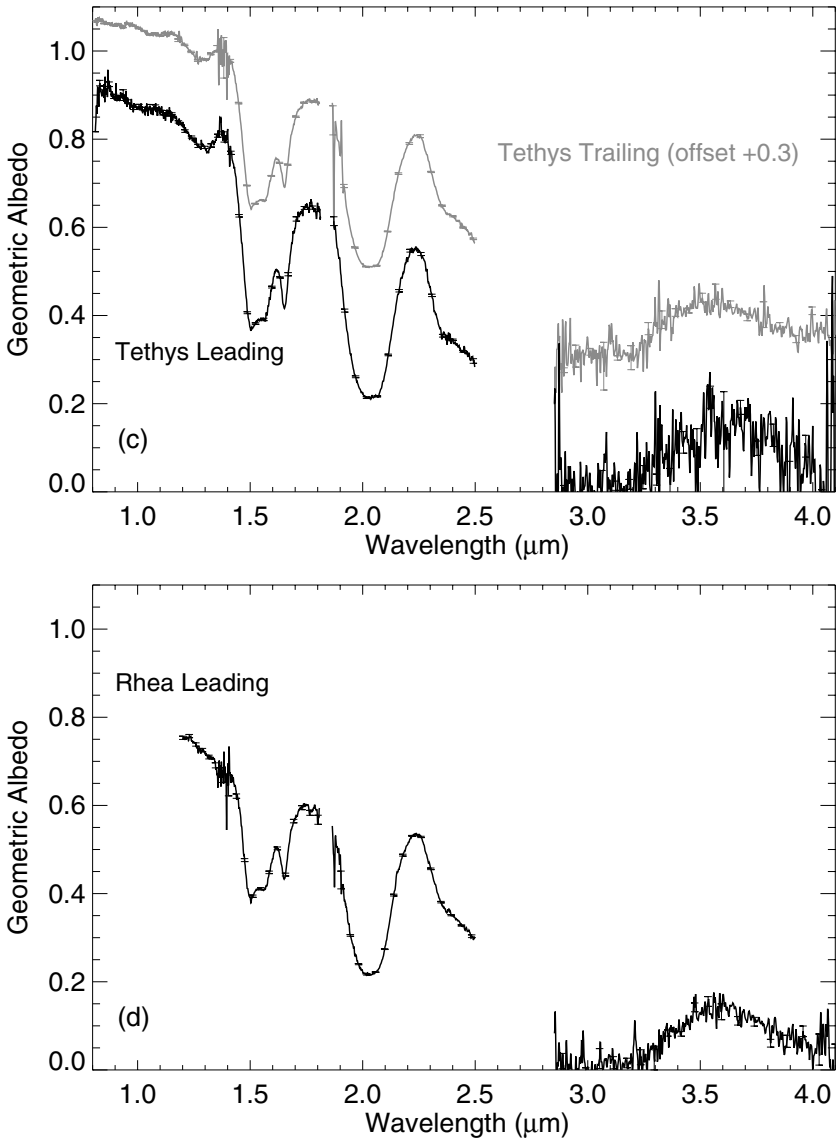

Fig. 1. continued.

Pang et al. 1984) particles, which should have short lifetimes ($\sim 10^4$ yr, Haff et al. 1983). Furthermore, the E-ring shows a peak in density at the orbit of Enceladus. It has therefore been suggested that perhaps the E-ring is a recent phenomenon associated with Enceladus, and that the event that created (is supplying?) the E-ring is also responsible for the photometrically uniform surface veneer (e.g., Morrison et al. 1984, and references therein).

The spectrum of Enceladus (Fig. 1b) has a very steep, blue slope at $\lambda < 1.4$ μm as compared to the other 3 satellites, yet the H_2O band depths are similar to the trailing sides of the other moons (see Table 2). This is consistent with the presence of a contaminant-free surface veneer. Close inspection of this spectrum reveals an apparent shallow absorption feature extending from about 2.235 to 2.265 μm (Fig. 2). This feature is very similar to the $\nu_2 + \nu_3$ and $\nu_2 + 2\nu_4$ combinations in NH_3, though the NH_3 absorptions extend to slightly shorter wavelengths than seen in the Enceladus spectrum. If this is NH_3 (or perhaps something closely related, such as an ammonia hydrate, ammonium hydroxide, etc.), then spectral modeling indicates that it is present in relatively small abundance (see Table 3, Fig. 2). The longitude of these observations is associated with the region identified as smooth plains, i.e. crater-free, in Voyager imagery, though our observations are at a more southerly latitude.

There are no signs of absorptions from any other minor components in this spectrum. CO_2 could comprise as much as 15 wt% and still not be detectible in these data, but the limits are more strict for CH_4 and CO.

3.3. Tethys

Tethys is the next classical satellite continuing outward from Enceladus, and it is significantly larger than Mimas and Enceladus (R = 530 km). Tethys' surface is heavily cratered, including the 400-km-diameter Odysseus crater. A very large

Table 3. Abundance limits for possible ices.

Object	Species	Upper limits (wt%)	
		12.5 μm	200 μm
Mimas (L)	CO_2	10	30
	NH_3	0.3	2–3
	CH_4	2–5	10
	CO	2	7–10
Mimas (T)	CO_2	5	15–20
	NH_3	0.5	5
	CH_4	2–3	7
	CO	3	10–15
Enceladus (T)	CO_2	5	10–15
	NH_3	0.5[a]	3.0[a]
	CH_4	2	7
	CO	1.5	7
Tethys (L)	CO_2	3–4	10–12
	NH_3	0.3	2–3
	CH_4	3	8–10
	CO	3	10–15
Tethys (T)	CO_2	1.5	5–7
	NH_3	0.2	2
	CH_4	1	5
	CO	1	5
Rhea (L)	CO_2	3	10
	NH_3	0.2	2–3
	CH_4	1–2	5–7
	CO	1	5

[a] Possible detection of NH_3 on Enceladus.

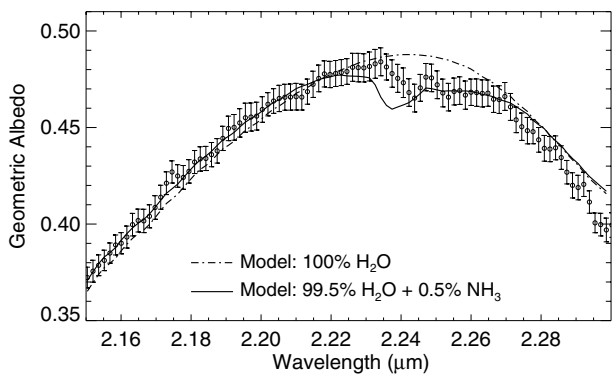

Fig. 2. A close look at the spectrum of Enceladus reveals spectral activity near 2.24 μm. The data deviate from the spectrum of pure water ice from about 2.235 to 2.265 μm. Mixing a small amount of NH_3 with the water ice creates a similar deviation. The optical constants used for the model calculations are from Grundy & Schmitt (1998) for H_2O (at 100 K) and Sill et al. (1981) for NH_3.

fracture, Ithaca Chasma, extends about three-quarters of the way around a great circle roughly centered on Odysseus. Crater counts of Plescia & Boyce (1982, 1983) indicate that part of the trailing hemisphere may be less heavily cratered than the rest of the surface. Voyager images did not reveal any dark/bright lineations as were visible in images of Dione & Rhea (Morrison et al. 1984). The leading hemisphere of Tethys is about 10–15% brighter than the trailing hemisphere (Buratti et al. 1990, 1998).

Our spectra of Tethys cover the range 0.8–4.1 μm for both the leading and trailing hemispheres (Fig. 1c). Along with being higher albedo, the leading side of Tethys has a steeper slope at $\lambda < 1.4$ μm than the trailing side. The H_2O bands at 1.25, 1.52, 2.02, and 3.0 μm are also *deeper* on the leading side than the trailing side. The 1.04 μm band, however, seems to be *less deep* on the leading side. This is all qualitatively consistent with fewer contaminants on the leading side.

No species were detected aside from H_2O. The data at $\lambda < 2.5$ μm have very high S/N, so constraints on abundances of minor species are stronger than for the Mimas and Enceladus data. There can be no more than 2 wt% NH_3 on Tethys. CO_2 could still comprise as much as 10 wt% and not be observable in these data. The 3- to 4-μm region provides an opportunity for a sensitive search for dark, organic material. These materials often exhibit absorptions in this region due to fundamental vibrational modes (e.g. C−H, O−H, C−C, S−H, N−H, N−O). The H_2O bands are saturated in this region. The trailing side spectrum has higher S/N than the leading side spectrum, and the Fresnel peak is visible near 3.1 μm, in the deepest part of the H_2O fundamental. There is no sign of any other components. Further ground-based observations dedicated to these objects can spend more integration time to obtain higher sensitivity data in this range and provide a more sensitive search for minor components.

3.4. Rhea

Rhea is the largest (R = 765 km) and the outer-most satellite addressed in this study (orbiting outside Tethys & Dione). The plasma environment is somewhat different at this radial distance than for the inner satellites, which could potentially lead to different chemical pathways for any chemistry induced by magnetospheric-particle impact (Delitsky & Lane 2002). The surface of Rhea is heavily cratered. Plescia & Boyce (1982) found a relatively complicated crater distribution; an absence of craters >30 km near the north pole and near the equator on the leading side, and a subdued topography with a dearth of small (<10 km) craters in other parts of the equatorial region. Some of the craters have bright patches on their walls, possibly similar to those recently seen on Phoebe by Cassini (Cassini press release PIA06075; Porco et al. 2004; Clark et al. 2004), which may be patches of exposed ice. The leading side of Rhea is brighter (by 15–20%, Buratti et al. 1990; Verbiscer & Veverka 1989) and more photometrically uniform than the trailing side. Despite the overall darker appearance, the trailing side contains bright streaks. These do not seem to occur in radial patterns or center on impact craters; their origin and nature remain uncertain.

Our Rhea spectrum extends to 4.1 μm (Fig. 1d). The short wavelength ($\lambda < 1.9$ μm) portion of this spectrum seems to suffer from a systematic error. This region was collected with the SXD mode of SpeX, with the spectrum consisting of six orders cross dispersed on the chip. At $\lambda < 1.2$ μm, these

orders were visibly "humped" relative to one another, and the overlap regions crisscrossed rather than lining up. We therefore omitted this region from the spectrum. Since it was collected at the same time with the same instrument, the 1.2–1.8 μm region may also suffer. Indeed, the 1.25- and 1.52-μm band depths seem anomalously low compared to the other bands in the Rhea spectrum and compared to the other satellites. The $\lambda > 1.9$ μm portion was collected separately with the LXD mode and showed no evidence of any problems.

There is no evidence in this spectrum for any minor components. No more than 2 wt% NH_3 is possible. The surface could contain at most about 10 wt% CO_2. The data at $\lambda > 2.8$ μm have relatively high S/N. The Fresnel peak is once again visible near 3.1 μm, but there is no sign of any other absorption aside from H_2O.

4. Discussion

4.1. Ammonia on Enceladus

A small feature in the Enceladus spectrum near 2.25 μm may be indicative of NH_3 ice or possibly an ammonia-hydrate on the surface. A possible feature near 2.0 μm in the same spectrum is in the same location as the $\nu_3 + \nu_4$ combination mode of NH_3, supporting the identification of ammonia in the spectrum. However, it is difficult to match both features simultaneously with mixing models. The shorter wavelength feature is in the middle of a strong H_2O band. Since the absorption coefficient of H_2O is much stronger here than near 2.25 μm, H_2O is more dominant in the mixture near 2.0 μm, and a larger amount of NH_3 is required to get a noticeable feature. The NH_3 band near 2.0 μm is also somewhat broader than the possible feature in the telescopic data. Further complicating the interpretation, the ~2.25-μm absorption band in the data of Enceladus is at a slightly longer wavelength than those in NH_3 ice, NH_3 hydrate, or NH_4OH (Cruikshank et al. 2005, their Table 4).

Some hydrated silicates (e.g., chlorite) also exhibit absorption features near 2.25 μm. We have been able to roughly fit the 2.25-μm feature in the Enceladus spectrum with 10 wt% chlorite mixed with H_2O ice. Whereas this mixture can approximately fit the K-band data, such a large amount of silicate material significantly darkens the spectrum at shorter wavelengths. The high albedo of Enceladus constrains the amount of such dark contaminants to much less than 1 wt% (cf. Clark et al. 1984b). Although we have considered two formes of mixtures of NH_3 and H_2O, ammonia molecules on Enceladus may be complexed with water ice in different proportions and physical configurations that would result in a band wavelength shift of the magnitude we observe. A similar effect occurs for the CO_2 absorption band observed on the Galilean satellites (Hibbitts et al. 2003) and Phoebe (Clark et al. 2004). Additional laboratory spectroscopic experiments with NH_3 and H_2O may be useful in exploring this possibility. Ammonia, or some related material, remains the most reasonable explanation for the spectral features we identify.

The possible identification of NH_3 on the surface of Enceladus could resolve a long standing puzzle concerning recent geologic activity on this moon. Voyager revealed regions of the surface that are entirely devoid of craters at the image resolution, suggesting a very recent resurfacing event (Smith et al. 1982). However, temperatures are too low in the Saturn system for cryovolcanism of pure H_2O, and Enceladus is not in a strong orbital resonance that would supply enough heating from tidal forces (Ellsworth & Shubert 1983; Squyres & Croft 1986; Greenberg 1984). The presence of ammonia and/or ammonia hydrates would lower the melting temperature sufficiently to allow cryovolcanic activity (Squyres & Croft 1986). NH_3 related condensates are cosmochemically likely constituents in the Saturnian sub-nebula (e.g. Pollack & Consolmagno 1984). This material should be detected by Cassini VIMS, which will also be able to map its spatial distribution on Enceladus. If the NH_3 is the catalyst for cryovolcanic activity, we would expect it to be associated with the smooth, crater-free plains.

As stated above, the possible feature we identify does not coincide exactly with an obvious candidate material. Furthermore, Cruikshank et al. (2005) also present K-band spectra of the trailing side of Enceladus obtained in 1995 and 1998 with comparable sensitivity that do not show evidence of spectral activity near 2.25 μm. The sub-observer longitudes they observed differed from ours by ~50° (267° and 275° compared to 320°), so there is a possibility that we are detecting a very localized deposit. Another possibility could be emplacement of material subsequent to their observations. Both of these possibilities are speculative, and the observations require confirmation. Fortunately, this confirmation (or refutation) will come relatively soon, as Cassini-VIMS continues to observe the Saturn system.

4.2. Grain size and contaminants

The brightness, spectral slope (0.9–1.4 μm), and band depths of H_2O dominated surfaces are all affected by both grain size and the presence of dark contaminants. In general, increasing the amount of dark contaminants will lower the albedo, flatten the spectral slope, and decrease the depths of the absorption bands, as long as the bands are not saturated. Larger grain sizes will also tend to lower the albedo, but will steepen the spectral slope and increase the depth of the absorption bands (see Fig. 3; Clark & Lucey 1984; Clark 1981). For saturated bands the band depth trend is reversed, such that more contaminants will increase the band depth and larger grains will decrease it. Based on their morphology, we do not believe that the bands at $\lambda < 2.5$ μm are saturated, so the former trends should hold. Combining the effects of grain size and contaminants can produce more complicated results (e.g., depths of some band increasing while others decrease).

The leading side of Mimas has a slightly lower albedo than the trailing side, as well as a flatter spectral slope and significantly deeper H_2O bands. The deeper absorption bands and lower albedo are consistent with larger grain sizes on the leading side, but the flatter spectral slope implies a larger amount of contaminants. It therefore seems likely that the leading side of Mimas has larger grains and contains slightly more contaminants than the trailing side. The leading side of Enceladus is also darker than its trailing side, but band depths

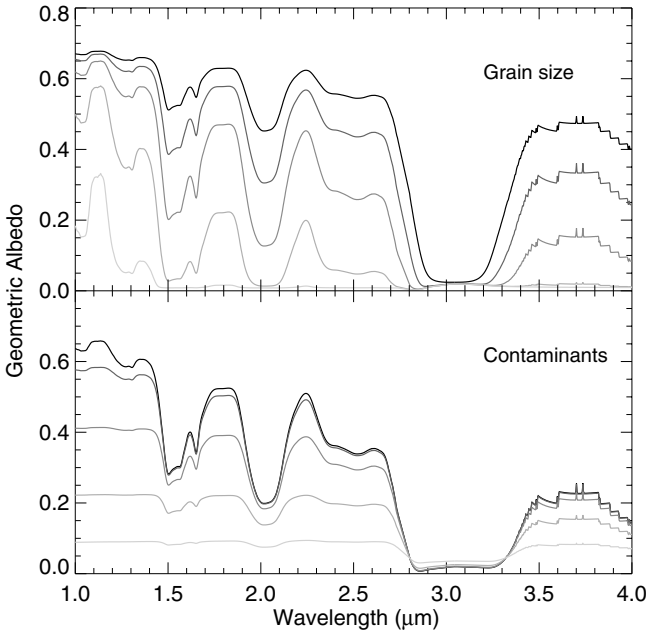

Fig. 3. Varying grain size and levels of dark contaminant both have a strong effect on the spectrum of H_2O. Hapke model calculations of water ice spectra demonstrate these effects. In the top frame, grain sizes of the curves are 2.5, 10, 50, 500, and 10 000 μm from top to bottom (dark to light). Increasing grain size darkens the spectrum, increases the spectral slope (1.0−1.4 μm), and increases band depths (until saturation, after which depths decrease). In the bottom frame, mixing ratios of dark contaminants of the curves are 0.01, 1.0, 10, 40, 80% from top to bottom (dark to light) for a grain size of 25 μm. Increasing the amount of opaque material darkens the spectrum, decreases the spectral slope, and decreases the band depth. We use amorphous carbon as the opaque material, and assume a temperature of 100 K for the H_2O ice. Optical constants are from Hudgins et al. (1993) for H_2O at $\lambda > 2.7$ μm, Grundy & Schmitt (1998) for H_2O at $\lambda < 2.7$ μm, and Rouleau & Martin (1993) for amorphous carbon. The apparent stepping at $\lambda > 3.4$ μm is an artifact of the precision of the optical constants and is not a real feature of H_2O.

and spectral slope for the leading side are not available for comparison with those presented in this paper.

Tethys shows somewhat different trends. The leading side has a higher albedo, steeper spectral slope, and slightly deeper H_2O bands than the trailing side. The band depths at 1.04 μm are similar to one another within the probable error of the measurements (~0.005). This behavior is consistent with similar grain sizes for both hemispheres, but fewer dark contaminants on the leading side. From data presented in Buratti et al. (1998) and Clark et al. (1984b), it seems that Dione and Rhea may share similar leading/trailing trends to Tethys.

Clark et al. (1984a,b) attribute leading/trailing H_2O band depth trends for icy Galilean and Saturnian satellites to magnetospheric particle bombardment. The impacting particles will sputter away the smaller grains, leaving a surface with larger grains than otherwise stable. Since Jupiter and Saturn (and therefore their magnetospheres) rotate faster than their satellites orbit, the bombardment is on the trailing sides of the moons. So, if this scenario were correct, the trailing sides of icy satellites of Saturn should have larger grains than their leading sides. This does not seem to be entirely consistent with the current data for either Tethys or Mimas.

Rather than larger grains on the trailing side, the Tethys data seem to imply more contaminants on this side, with similar (or maybe slightly larger) grains. This situation might also arise from magnetospheric particle bombardment. If impact gardening would replenish the small grain sizes on a faster or similar timescale than sputtering removed them, then the grain size distribution would not be appreciably different on the trailing side as compared to the leading side. Bombardment of the trailing side by magnetospheric particles might still drive chemistry (e.g., Delitsky & Lane 2002) that could lead to more contaminants on that side. Dione and Rhea could be affected similarly. The higher proton flux at Dione than at Tethys as reported by Van Allen et al. (1980) and reproduced by Clark et al. (1984b) might explain the larger hemispheric dichotomy on Dione.

Mimas, on the other hand, appears to have both larger grains and slightly more contaminants on the *leading* side. This is not consistent with bombardment of the trailing side by magnetospheric particles. Mimas orbits within the inner edge of the E-ring, and just outside the A-ring. Sputtering of the leading side of Mimas by small, dark ring particles could explain both the larger grains and the presence of contaminants. Enceladus and Tethys also orbit within the E-ring. Enceladus may show similar trends to Mimas, but not enough data are available to make a determination. Also, the surface properties of Enceladus may be controlled or at least affected by recent geological activity. Tethys orbits near the outer edge of the E-ring, and far from the other rings. Magnetospheric effects could dominate effects of ring particle bombardment at Tethys distance.

Hamilton & Burns (1994) proposed a scenario in which the E-ring is self-sustaining. Radiation pressure perturbs ring particles (~1 μm in size) into highly eccentric orbits. Particle collisions with Enceladus launch an equal or larger number of similar sized particles into orbit. A by-product of this model is that eccentric E-ring particles preferentially impact the trailing side of Mimas and the leading side of Tethys and Dione. If these impacts of small ice particles on icy surfaces result in higher albedo and smaller particles (on the surface), then this scenario could also explain the observed spectral/photometric trends.

4.3. Upper limits on selected ices

Using radiative transfer scattering theory (e.g., Hapke 1993), we have estimated upper limits to the amounts of four ices on the surfaces of these four moons. Because each of these ices (NH_3, CO_2, CH_4, and CO) exhibit diagnostic absorptions in the *K*-band region, and because our data of all four satellites have high S/N in this range, we use this spectral range for the estimates of upper limits. Figures 2 and 4 illustrate the absorptions expected from small amounts of NH_3, CO_2, and CH_4 (see also Cruikshank et al. 2005, their Figs. 5–7). CO is not shown, but it exhibits a single absorption in the *K*-band, at 2.35 μm. In these models, we assume intimate granular (salt and pepper) mixing, where grains of differing materials are mixed together; e.g., a regolith. Other types of mixtures, however, could result

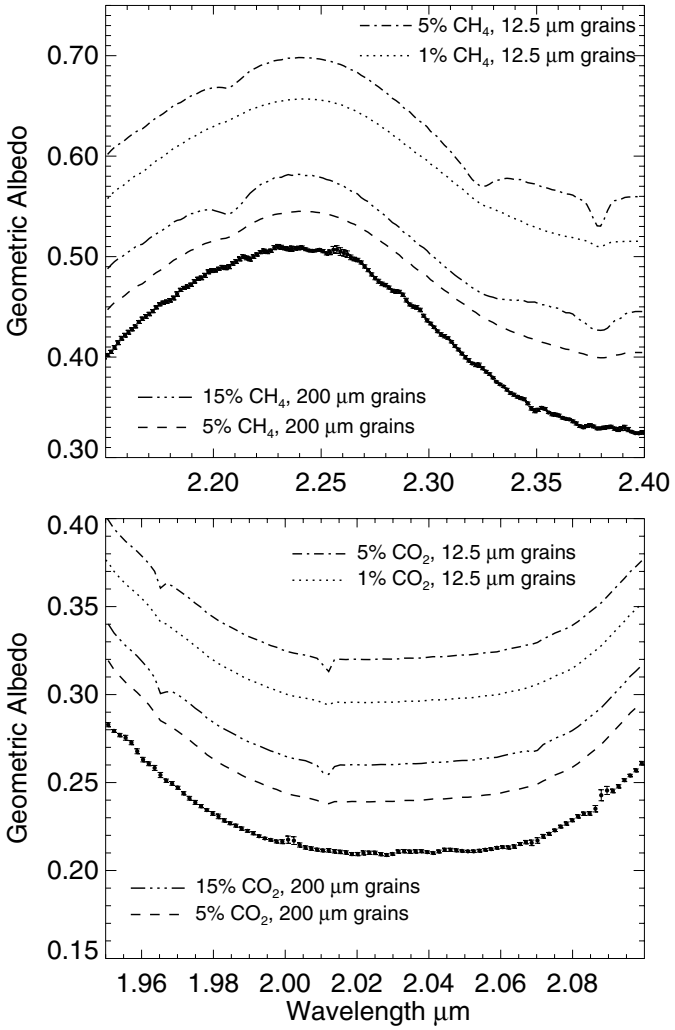

Fig. 4. Portions of the spectrum of the trailing side of Tethys (filled circles) are shown with mixtures of H_2O with small amounts of CH_4 (*top*) and CO_2 (*bottom*). The H_2O grain size is set at 20 μm to fit the full *K*-band segment of Tethys' spectrum. To estimate upper limits, the amount of the contaminant is increased until at least one absorption band is larger than the noise in the data. The CH_4 bands in this region are at 2.21, 2.32, and 2.38 μm. The CO_2 bands are at 1.97, 2.01 and 2.07 μm.

in very different upper limits. For example, minor constituents mixed within a H_2O grain (e.g., trace molecules dissolved in large, transparent crystals) can produce a stronger signature at much lower concentration levels (e.g., Poulet et al. 2002). This occurs because the minor constituent can significantly increase the absorption coefficient of the surface grain in the spectral region of its absorption bands. We do not address this type of intra-particle mixing in this work. The upper limits we list in Table 3 are only applicable to the assumption of salt and pepper type mixing.

Since we interpret the Enceladus spectrum as possibly showing NH_3, the level listed in Table 3 is a detected level rather than an upper limit. No other non-H_2O ices were detected on this or the other moons, and NH_3 was also not detected on the other three moons. The limits on NH_3 are quite strict for Mimas, Tethys, and Rhea. If NH_3 is part of the bulk composition and drives cryovolcanism, then this is consistent with a lack of young (lightly cratered) terrain on any of these moons. Methane and CO are very volatile, and would not survive long on the surfaces of these moons. The non-detection of these two ices is therefore not surprising. CO_2 has been detected by Cassini VIMS on both Phoebe and Iapetus (Cassini press release PIA06400; Clark et al. 2004; Buratti et al. 2004) by the strong fundamental stretch absorption at 4.26 μm. It is present in low abundances, seems to be correlated with lower albedo, H_2O-poor regions, and has been interpreted as fluid or gaseous inclusions in minerals from a slight shift in the wavelength of the detected band. Our upper limits on CO_2 are not very strict, so upcoming data from Cassini may yet reveal its presence on the four moons in this study as well.

4.4. Other minor constituents

We discussed above the effects that sputtering due to bombardment by energetic magnetospheric particles can have on the spectral properties (brightness, spectral slope, band depths) of an icy surface. Chemistry induced by the impact and implantation of magnetospheric ions can also be important. Delitsky & Lane (2002) suggested chemical pathways that could be exploited in the saturnian system and the species that would result. These include NO, NO_2, HNO, HNO_2, NH_4OH, N_2O, HNO_3, HCO, HNCO, H_2O_2, O_2, O_3, as well as many organic molecules. Many of these species are active in the infrared and would be observable at VIMS wavelengths if present in sufficient amounts (Delitsky & Hibbits 2004). We have not performed quantitative upper limit calculations for all these molecules, but we see no evidence for any of them in the data.

Organic material may also be created by the irradiation of ices by UV photons or cosmic rays (e.g., Thompson et al. 1987; Allamandola et al. 1988; Bohn et al. 1994). There are albedo variations on the surfaces of the icy satellites of Saturn, which may be (at least in part) due to such radiolytic products. Organic molecules exhibit strong fundamental absorptions in the 3.2–3.4 μm region, as well as overtones and combinations at shorter wavelengths. We see no evidence for any such absorptions in these data. If the darker terrains are due to radiolytic organics, perhaps the abundance is too small (< about a few wt%) to be detected. Clark et al. (2004) attribute some small absorptions in the Cassini VIMS spectrum of Pheobe to organics. Further observations of the other moons at the high spatial resolutions possible with VIMS may reveal similar deposits on the other moons.

5. Conclusions

These recent spectra of four icy moons of Saturn provide context for ongoing observations of this system by Cassini. We have measured the highest sensitivity data to date for all four objects, and extended the spectral coverage to 4.1 μm for Tethys and Rhea.

We report a possible detection of NH_3 (or a closely related material) on the trailing hemisphere of Enceladus, corresponding with the crater free smooth plains unit imaged by Voyager. It has been expected that ammonia or ammonia-hydrate would

be a necessary component to help drive the geological activity inferred from Voyager imagery (e.g., Ellsworth & Shubert 1983). Our results may be the first confirmation of this hypothesis. If real, this feature should be detected by VIMS on Cassini, which will also have the capability of mapping its spatial distribution. There are no indications of any other minor components in any of the spectra.

The H_2O band depths are fairly similar among these four moons, but leading/trailing differences vary somewhat. These variations may be due to differing irradiation environments/sources for the inner moons (Enceladus and Mimas) than for the outer moons (Tethys, Dione, Rhea). Ongoing quantitative analysis of the H_2O band shapes will help constrain physical properties of the surface grains (e.g., particle size, temperature), and will provide a more rigorous search for any non-H_2O components that may be affected the band shapes.

Delitsky & Lane (2002) predicted surface chemistry driven by interactions with the magnetosphere. The chemistry they suggest must not produce non-H_2O ices in sufficient quantity to be detected in our data ($\lesssim$1–10 wt%). VIMS detected CO_2 on the surface of Pheobe during the flyby of that small moon just before orbit insertion (Cassini press release PIA06400). If CO_2 is also present on the other satellites, it must occur in small abundances.

Acknowledgements. We greatly appreciate observing assistance by Matt Chamberlain, David O'Brien, and John Weirich, and a helpful review by Dr. Bonnie Buratti. We also thank the staff of the NASA Infrared Telescope Facility, which is operated by the University of Hawaii under Cooperative Agreement No. NCC 5-538 with the National Aeronautics and Space Administration, Office of Space Science, Planetary Astronomy Program.

References

Allamandola, L. J., Sandford, S. A., & Valero, G. J. 1988, Icarus, 76, 225
Bohn, R. B., Sandford, S. A., Allamandola, L. J., & Cruikshank, D. P. 1994, Icarus, 111, 151
Bridge, H. S., Belcher, J. W., Lazarus, A. J., et al. 1981, Science, 212, 217
Bridge, H. S., Bagenal, F., Belcher, J. W., et al. 1982, Science, 215, 563
Buratti, B. J. 1988, Icarus, 75, 113
Buratti, B. J., & Veverka, J. 1984, Icarus, 58, 254
Buratti, B. J., Mosher, J. A., & Johnson, T. V. 1990, Icarus, 87, 339
Buratti, B. J., Mosher, J. A., Nicholson, P. D., & McGhee, C. A. 1998, Icarus, 136, 223
Buratti, B. J., Cruikshank, D. P., Clark, R. N., et al. 2004, Bull. Am. Astron. Soc., 36, 1073 (Abstract #4.09)
Cassini press release PIA06075, `http://saturn.jpl.nasa.gov`
Cassini press release PIA06400, `http://saturn.jpl.nasa.gov`
Clark, R. N. 1981 J. Geophys. Res., 86, 3087
Clark, R. N., & Lucey, P. G. 1984, J. Geophys. Res., 89, 6341
Clark, R. N., Fanale, F. P., & Zent, A. P. 1984a, Icarus, 56, 233
Clark, R. N., Brown, R. H., Owensby, P. D., & Steele, A. 1984b, Icarus, 58, 265
Clark, R. N., Brown, R. H., Jaumann, R., et al. 2004, Bull. Am. Astron. Soc., 36, 1070 (Abstract #4.01)
Cruikshank, D. P. 1980, Icarus, 41, 246
Cruikshank, D. P., & Brown, R. H. 1982, Icarus, 50, 82
Cruikshank, D. P., Veverka, J., & Lebofsky, L. A. 1984, in Saturn, ed. T. Gehrels, & M. S. Matthews, 640
Cruikshank, D. P., Owen, T. C., Dalle Ore, C., et al. 2005, Icarus, in press
Delitsky, M. L., & Lane, A. L. 2002, J. Geophys. Res., 107(E11), 5093
Delitsky, M. L., & Hibbitts, C. A. 2004, Bull. Am. Astron. Soc., 36, 1124 (Abstract #24.06)
Ellsworth, K., & Schubert, G. 1983, Icarus, 54, 490
Emery, J. P. 2002, Ph.D. Thesis, Univ. Arizona
Emery, J. P., & Brown, R. H. 2003, Icarus, 164, 104
Eviatar, A. 1984, J. Geophys. Res., 89, 3821
Fink, U., Larson, H. P., Gautier III, T. N., & Treffers, R. R. 1976, ApJ, 207, L63
Frank, L. A., Burek, K. L., Ackerson, J. H., et al. 1980, J. Geophys. Res., 85, 5695
Greenberg, R. 1984, in Saturn, ed. T. Gehrels, & M. S. Matthews, 593
Grundy, W. M., & Schmitt, B. 1998, J. Geophys. Res., 103, 25 809
Grundy, W. M., Buie, M. W., Stansberry, J. A., & Spencer, J. R. 1999, Icarus, 142, 536
Haff, P. K., Eviatar, A., & Siscoe, G. L. 1983, Icarus, 56, 426
Hamilton, D. P., & Burns, J. A. 1994, Science, 264, 550
Hapke, B. 1993, Theory of reflectance and emittance spectroscopy (Cambridge Univ. Press)
Hibbitts, C. A., Pappalardo, R. T., Hansen, G. B., & McCord, T. B. 2003, JGR(E5), 108, 2-1
Hudgins, D. M., Sandford, S. A., Allamandola, & L. J., Tielens, A. G. G. M. 1993, ApJS, 86, 713
Johnson, T. V., Veeder, G. J., & Matson, D. L. 1975, Icarus, 24, 428
Krimigis, S. M., Carbary, J. F., Keath, E. P., et al. 1983, J. Geophys. Res., 88, 8871
Momary, T. W., Baines, K. H., Yanamandra-Fisher, P. A., et al. 2000, Icarus, 148, 397
Morrison, D., Cruikshank, D. P., Pilcher, C. B., & Rieke, G. H. 1976, ApJ, 207, L213
Morrison, D., Johnson, T. V., Shoemaker, E. M., et al. 1984, in Saturn, ed. T. Gehrels, & M. S. Matthews, 609
Morrison, D., Owen, T., & Soderblom, L. A. 1986, in Satellites, ed. J. Burns, & M. S. Matthews, 764
Owen, T. C., Cruikshank, D. P., Dalle Ore, C. M., et al. 1999, Icarus, 140, 379
Pang, K. D., Voge, C. C., Rhoads, J. W., & Ajello, J. M. 1984, J. Geophys. Res., 89, 9459
Passey, Q. R. 1983, Icarus, 53, 105
Plescia, J. B., & Boyce, J. M. 1982, Nature, 295, 285
Plescia, J. B., & Boyce, J. M. 1983, Nature, 301, 666
Pollack, J. B., & Consolmagno, G. 1984, in Saturn, ed. T. Gehrels, & M. S. Matthews, 811
Porco, C. C., & Cassini Imaging Team 2004, Bull. Am. Astron. Soc., 36, 1019 (Abstract #1.02)
Poulet, F., Cuzzi, J. N., Cruikshank, D. P., et al. 2002, Icarus, 160, 313
Rayner, J. T., Toomey, D. W., Onaka, P. M., et al. 1998, Proc. SPIE, 3354, 468
Rouleau, F., & Martin, P. G. 1993, ApJ, 377, 526
Sill, G., Fink, U., & Ferraro, J. R. 1980, J. Opt. Soc. Am., 70, 724
Smith, B. A., Soderblom, L., Batson, R. M., et al. 1982, Science, 215, 504
Squyres, S. W., & Croft, S. K. 1986, in Satellites, ed. T. Gehrels, & M. S. Matthews, 293
Thompson, W. R., Murray, B. G. J. P. T., Khare, B. N., & Sagan, C. 1987, J. Geophys. Res., 92, 14 933
Van Allen, J. A., Thomsen, M. F., Randall, B. A., et al. 1980, Science, 207, 415
Verbiscer, A. J., & Veverka, J. 1989, Icarus, 82, 336
Verbiscer, A. J., & Veverka, J. 1992, Icarus, 99, 63